# Supporting Information

## Keplerate-type polyoxometalate {$Mo_{72}Fe_{30}$} nanoparticle anodes for high-energy lithium-ion batteries

Shao-Chu Huang,[a] Chia-Ching Lin,[a] Chi-Ting Hsu,[a] Chun-Han Guo,[a] Tsan-Yao Chen,[b] Yen-Fa Liao,[c] and Han-Yi Chen[a]*

*[a] Department of Materials Science and Engineering, National Tsing Hua University, 101, Sec. 2, Kuang-Fu Road, Hsinchu 30013, Taiwan*
*[b] Department of Engineering and System Science, National Tsing Hua University, 101, Sec. 2, Kuang-Fu Road, Hsinchu 30013, Taiwan*
*[c] National Synchrotron Radiation Research Center, 101 Hsin-Ann Road, Hsinchu, 30013, Taiwan*
** Corresponding author: Prof. Han-Yi Chen (hanyi.chen@mx.nthu.edu.tw)*

**Table S1.** Summary of POMs as anode materials for LIBs

| Electrode | Current Density | 1st /2nd Charge/Discharge Capacity | Cycle Number (Retention %) | Ref. |
|---|---|---|---|---|
| $H_5PMo_{10}V_2O_{40}$/MOF[a)]/RGO | 50 mA $g^{-1}$ | 2368/1300 | 100th (~82.6) | 1 |
| EMI[b)]-$Mo_{72}V_{30}$@rGO | 100 mA $g^{-1}$ | 2046/1200 | 100th (~100) | 2 |
| $Na_3[AlMo_6O_{24}H_6]$-EDAG[c)] | 100 mA $g^{-1}$ | 1835/1180 | 100th (~84.1) | 3 |
| $\{[Co_3O(CH_3CO_2)_6(C_5H_5N)_3]^+\}_3[PMo_{12}O_{40}]^{3-}$/SWCNT[d)] | 100 mA $g^{-1}$ | 1469/1118 | 100th (~90.5) | 4 |
| $[(Bu_4N)_2[Mo_6O_{18}$-N-Ph[e)]-(o-$CH_3)_2$-p-SCN] | 50 mA $cm^{-2}$ | 1678/1050 | 100th (~85) | 5 |
| $H_2[Cu^{II}_4(Htrz)_5(H_2O)_2][Mo^{VI}_4Cu^{II}_4O_{26}]_{0.5}\cdot 3H_2O$ | 100 mA $g^{-1}$ | 1893/ 1005 | 200th (~69.7) | 6 |
| Py-Anderson[f)]-CNT | 0.1 mA $cm^{-2}$ | 1899/990 | 100th (~61.1) | 7 |
| $(nBu_4N)_3(DMA)[(MnCl)V_{12}O_{32}Cl]$/GQD[g)] | 100 mA $g^{-1}$ | 1645/985 | 100th (~98.5) | 8 |
| $(NH_4)_6P_2Mo_{18}O_{62}$/ GO-IL[h)] | 100 mA $g^{-1}$ | 1433/945 | 100th (~102) | 9 |
| $[PMo_{12}O_{40}]^{3-}$/PANI[i)]/MWNTs[j)] | 50 mA $g^{-1}$ | 1572/942 | 100th (~106) | 10 |
| $H_5PMo_{10}V_2O_{40}$/PDA[k)] | 100 mA $g^{-1}$ | activation/915 | 300th (~93) | 11 |
| $Na[Ag_{16}(Trz^{l)})_9(H_2O)_4][P_2W_{18}O_{62}]\cdot H_2O$ | 100 mA $g^{-1}$ | 1452/901 | 100th (~63.2) | 12 |
| $[Ag_{10}(trz)_4(H_2O)_2][HPW_{12}O_{40}]$/SWNT | 100 mA $g^{-1}$ | 2000/859 | 70th (~93.1) | 13 |
| $H_3[Ag_{27}(trz)_{16}(H_2O)_6][SiW_7^{VI}W_5^{V}O_{40}]_2\cdot 5H_2O$ | 50 mA $g^{-1}$ | 1356/832 | 100th (~54.8) | 14 |
| $[Cu_{18}(trz)_{12}Cl_3(H_2O)_2][PW_{12}O_{40}]$/ SWNT[d]–COOH | 100 mA $g^{-1}$ | 1298/809 | 170th (~97.1) | 15 |
| $[PMo_8^{V}Mo_4^{VI}O_{37}(OH)_3Zn_4][TPT^{m)}]_5\cdot 2TPT\cdot 2H_2O$ | 50 mA $g^{-1}$ | 1322/800 | 200th (~92.5) | 16 |
| $\{[Ni_6(OH)^{3-}(H_2O)(en^{n)})_3(PW_9O_{34})][Ni_6(OH)_3(H_2O)_4(en)_3(PW_9O_{34})](BDC^{o)})_{1.5}]\}[Ni(en)(H_2O)_4]\cdot H_3O$ | 1.25 C | 1421/780 | 500th (~48.7) | 17 |
| $Py–(Bu_4N)_4\{(SiW_{11}O_{39})[O(SiCH_2CH_2CH_2NH–COOCH_2C_{16}H_9)_2]\}$ /SWNTs | 0.5 mA $cm^{-2}$ | 1570/707 | 100th (~74) | 18 |
| $Na_7H_2[PV_{14}O_{42}]$ | 100 mA $g^{-1}$ | 961/687 | 150th (~80) | 19 |
| $(Bu_4N)_4\{(SiW_{11}O_{39})[O(SiCH_2CH_2CH_2NH_2\cdot HCl)_2]\}$/CNT[c)] | 0.5 mA $cm^{-2}$ | 1189/650 | 100th (~92.3) | 20 |
| **{$Mo_{72}Fe_{30}$}** | 100 mA $g^{-1}$ | 1437/1150 | 100th (92) | This work |

[a)]MOF: consists of $Cu^{2+}$ and 1,3,5-benzenetricarboxylic acid (HKUST-1); [b)]EMI: 1-ethyl-3-methylimidazolium; [c)]EDAG: ethylenediamine-decorated reduced graphene oxide; [d)]SWCNT/SWNT: single-walled carbon nanotubes; [e)]Ph: phenols; [f)]Py-Anderson: $[[N(n\text{-}C_4H_9)_4]_3[MnMo_6O_{18}\text{-}\{(OCH_2)_3CNH\text{-}CH_2\text{-}C_{16}H_9\}_2]]$; [g)]GQD: graphene quantum dot; [h)]GO-IL: graphene oxide-ionic liquid; [i)]PANI: polyaniline; [j)]MWNT: multi-walled carbon nanotubes; [k)]PDA: polydopamine; [l)]Trz: 1,2,3 triazole; [m)]TPT: tris-(4-pyridyl) triazine; [n)]en: ethylenediamine; [o)]BDC: H2BDC = 1,4-benzenedicarboxylic acid.

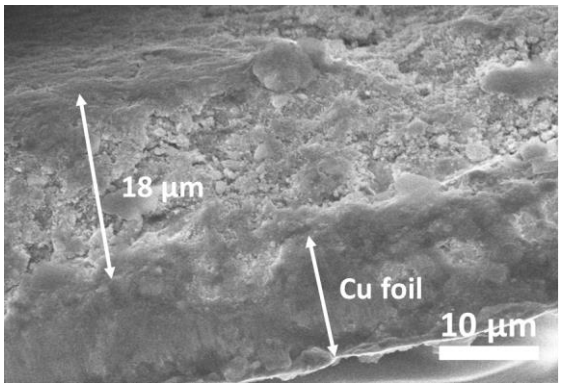


**Fig. S1** SEM cross section image of **{Mo$_{72}$Fe$_{30}$}** electrode

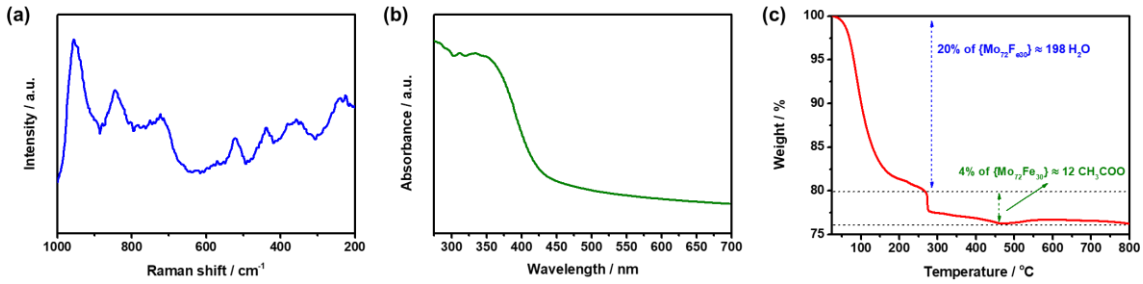


**Fig. S2** (a) Raman, (b) UV–Vis, and (c) TGA spectra of the **{Mo$_{72}$Fe$_{30}$}** powders.

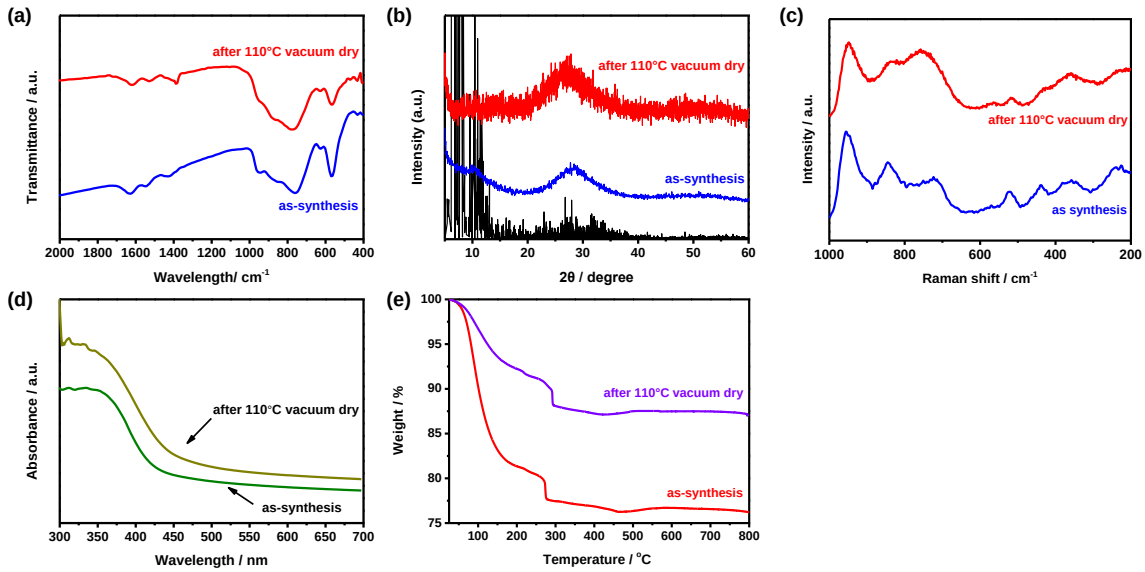


**Fig. S3** (a) FTIR spectrum, (b) XRD patterns (λ = 0.154 nm), (c) Raman, (d) UV–Vis, and (e) TGA spectra of the 110°C vacuum-dried **{Mo$_{72}$Fe$_{30}$}** powders.

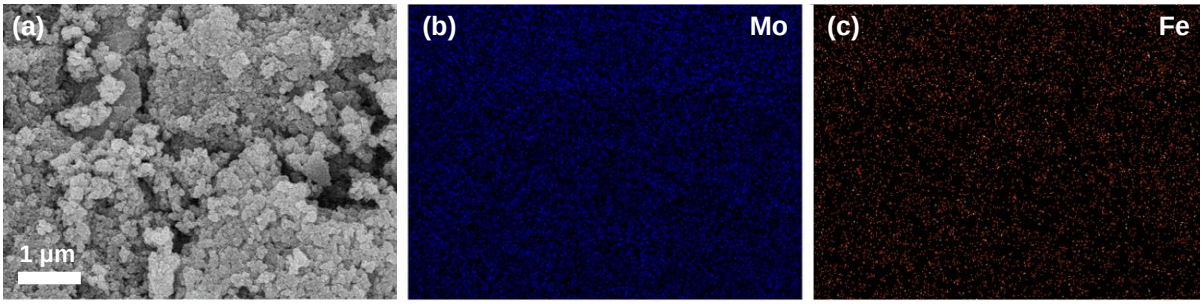


**Fig. S4** (a) SEM image, and EDS elemental mapping of the **{$Mo_{72}Fe_{30}$}** powder for (b) Mo and (c) Fe.

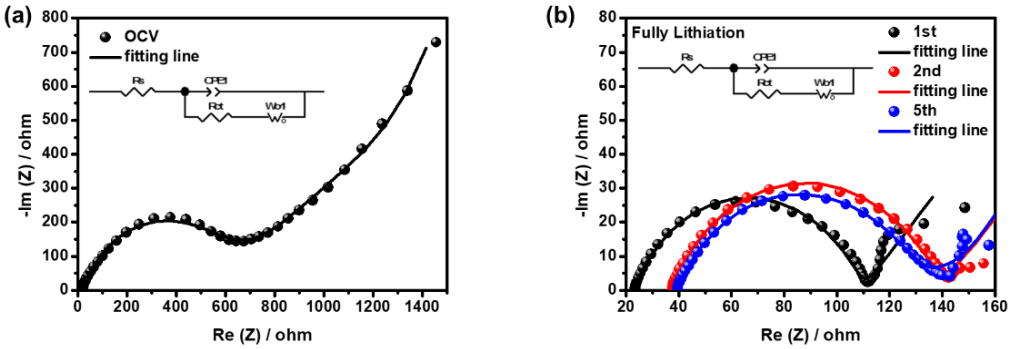


**Fig. S5** Nyquist plots of the {$Mo_{72}Fe_{30}$} electrodes at (a) OCV and (b) 0.01 V (fully lithiation) at the 1$^{st}$, 2$^{nd}$, and 5$^{th}$ cycles.

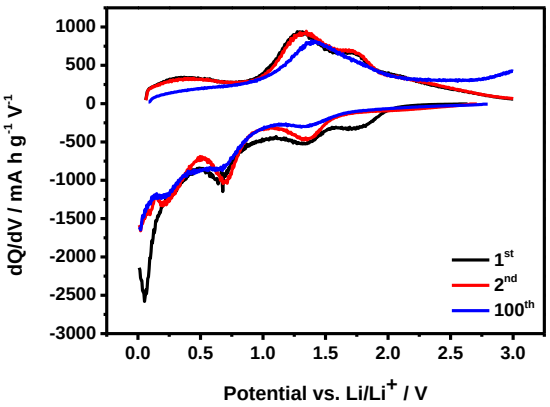


**Fig. S6** Differential capacity (dQ/dV) plots of the galvanostatic charge/discharge curves, at a current density of 100 mA g$^{-1}$.

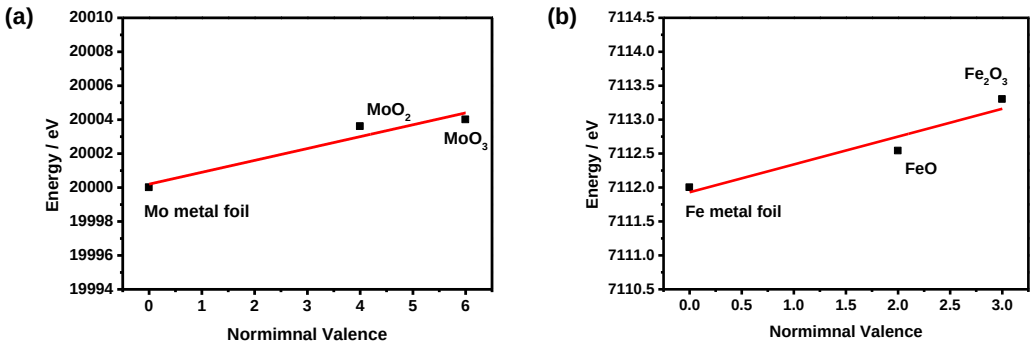


**Fig. S7** (a) Mo and (b) Fe valencies vs. the first peak value, in the derivative of energy, for the reference materials.

**Table S2.** R-factor of linear combination fitting for the **{$Mo_{72}Fe_{30}$}** powder

| Element | Potential | R-factor | Element | Potential | R-factor |
|---|---|---|---|---|---|
| Mo | OCV | 0.022 | Fe | OCV | 0.023 |
| | 1L | 0.002 | | 1L | 0.003 |
| | 1D | 0.018 | | 1D | 0.01 |
| | 2L | 0.001 | | 2L | 0.008 |

OCV: open-circuit voltage; 1L: the first full lithiation, at 0.01 V; 1D: the first full delithiation, at 3 V; and 2L: the second lithiation, at 0.01 V. R-factor $= \frac{\sum((data-fit)^2)}{\sum(data^2)}$

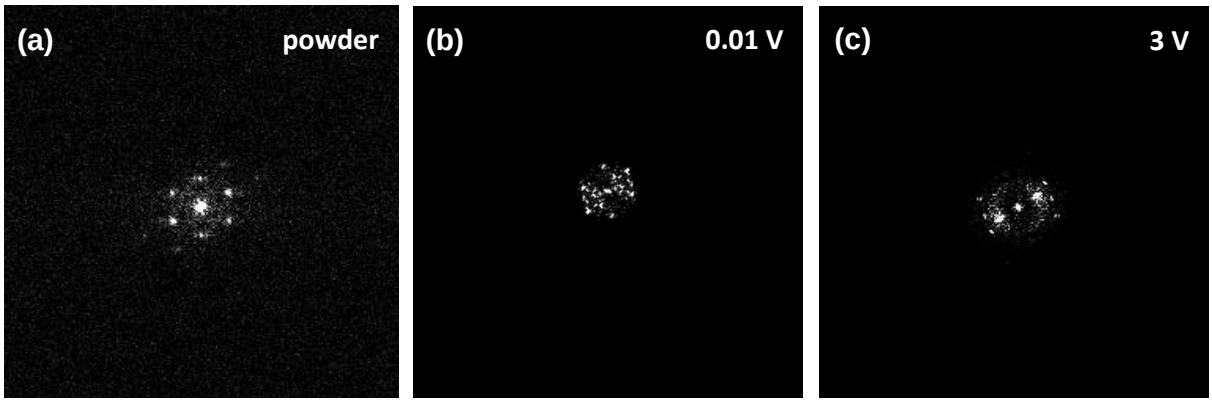


**Fig. S8** Corresponding Fourier Transform patterns of *ex situ* TEM images. (a) **{$Mo_{72}Fe_{30}$}** powder, (b) electrode at 1L, and (c) electrode at 1D.

**Table S3.** Mo K-edge EXAFS fitting parameters for the **{$Mo_{72}Fe_{30}$}** powder

| Path | *CN* [a)] | $\sigma^2$ (Å$^2$)[b)] | *R* (Å)[c)] | $E_0$ (eV) |
|---|---|---|---|---|
| Mo–O | 3.36 | 0.0028 | 1.72 | |
| Mo–O | 1.58 | 0.0029 | 1.79 | 2.71 |
| Mo–O | 0.77 | 0.0034 | 2.07 | |

[a)]coordination number. [b)]Debye–Waller factors. [c)]Bond length. [d)]Energy shift. R-factor of the fitting is 0.015. R-factor $= \frac{\sum_{i=1}^{N}[f(R_i)]^2}{\sum_{i=1}^{N}([\mathrm{Re}(\tilde{\chi}(R_i|data))]^2+[\mathrm{Im}(\tilde{\chi}(R_i|data))]^2)}$

**Table S4.** Fe K-edge EXAFS fitting parameters for the **{$Mo_{72}Fe_{30}$}** powder

| Path | *CN* [a)] | $\sigma^2$ (Å$^2$)[b)] | *R* (Å)[c)] | $E_0$ (eV) |
|---|---|---|---|---|
| Fe–O | | | 1.95 | |
| Fe–O | 1.77 | 0.0029 | 1.98 | -2.907 |
| Fe–O | | | 2.03 | |

[a)]coordination number. [b)]Debye–Waller factors. [c)]Bond length. [d)]Energy shift. R-factor of the fitting is 0.004. R-factor $= \frac{\sum_{i=1}^{N}[f(R_i)]^2}{\sum_{i=1}^{N}([\mathrm{Re}(\tilde{\chi}(R_i|data))]^2+[\mathrm{Im}(\tilde{\chi}(R_i|data))]^2)}$

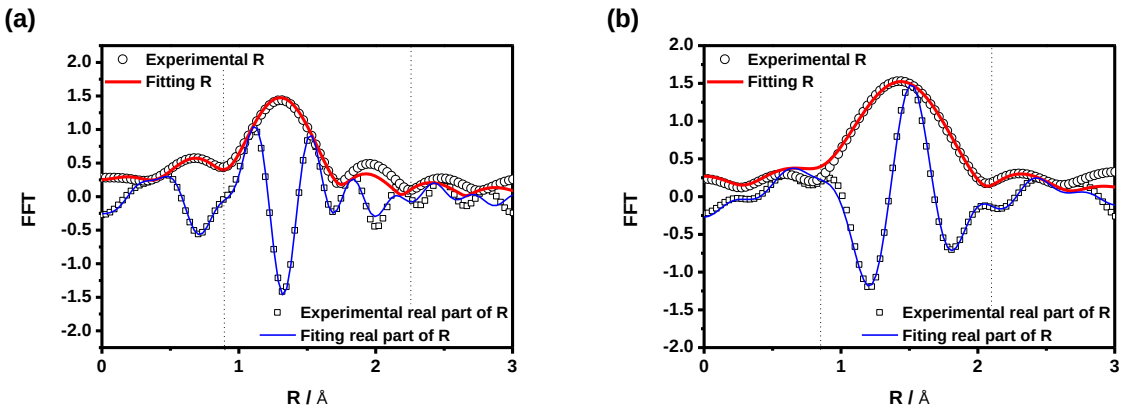


**Fig. S9** (a) Mo K-edge (b) Fe K-edge Fast FT (FFT)–EXAFS and the real part of the FFT–EXAFS experimental data and fitting curves of the **{$Mo_{72}Fe_{30}$}** powder.

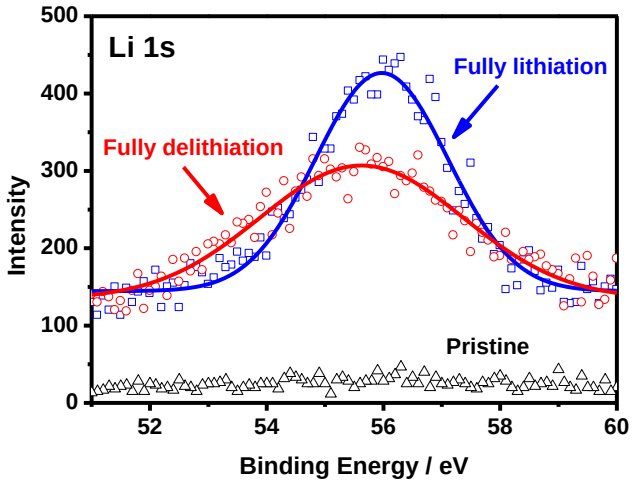


**Fig. S10** *Ex-situ* Li 1s XPS spectrum of the **{$Mo_{72}Fe_{30}$}** pristine electrode, electrode at 1L, and electrode at 1D.

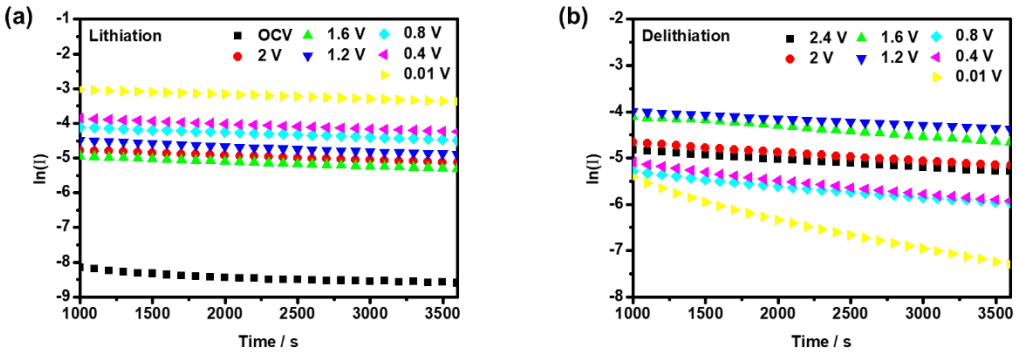


**Fig. S11** ln(I) vs. time in the (a) first discharge and (b) first charge processes of **{$Mo_{72}Fe_{30}$}**, as an anode for LIBs.

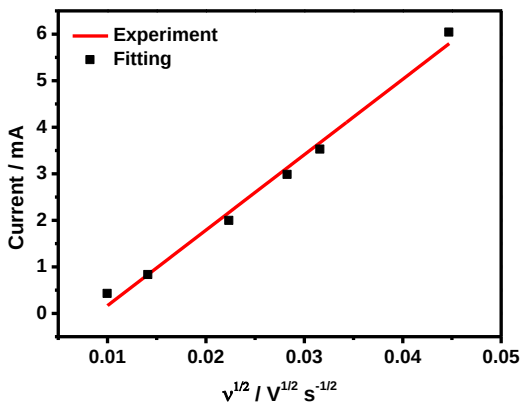


**Fig. S12** CV plot of current vs. scan rate

## References


1. H. Ying and W. Q. Han, *Advanced Science*, 2017, **4**, 1700298.
2. W.-J. Liu, G. Yu, M. Zhang, R.-H. Li, L.-Z. Dong, H.-S. Zhao, Y.-J. Chen, Z.-F. Xin, S.-L. Li and Y.-Q. Lan, *Small Methods*, 2018, **2**, 1800154.
3. J. Xie, Y. Zhang, Y. Han and C. Li, *ACS Nano*, 2016, **10**, 5304-5313.
4. B. Iqbal, X. Jia, H. Hu, L. He, W. Chen and Y.-F. Song, *Inorganic Chemistry Frontiers*, 2020, **7**, 1420-1427.
5. R. N. Nasim Khan, N. Mahmood, C. Lv, G. Sima, J. Zhang, J. Hao, Y. Hou and Y. Wei, *RSC Advances*, 2014, **4**, 7374-7379.
6. P. Zhu, X. Yang, X. Li, N. Sheng, H. Zhang, G. Zhang and J. Sha, *Dalton Transactions*, 2020, **49**, 79-88.
7. L. Huang, J. Hu, Y. Ji, C. Streb and Y.-F. Song, *Pyrene-Anderson-Modified CNTs as Anode Materials for Lithium-Ion Batteries*, 2015.
8. Y. Ji, J. Hu, J. Biskupek, U. Kaiser, Y.-F. Song and C. Streb, *Chemistry – A European*

*Journal*, 2017, **23**, 16637-16643.
9. J. Hu, H. Diao, W. Luo and Y.-F. Song, *Chemistry – A European Journal*, 2017, **23**, 8729-8735.
10. J. Hu, F. Jia and Y.-F. Song, *Chemical Engineering Journal*, 2017, **326**, 273-280.
11. Y.-H. Ding, J. Peng, S.-U. Khan and Y. Yuan, *Chemistry – A European Journal*, 2017, **23**, 10338-10343.
12. X.-Y. Yang, T. Wei, J.-S. Li, N. Sheng, P.-P. Zhu, J.-Q. Sha, T. Wang and Y.-Q. Lan, *Inorganic Chemistry*, 2017, **56**, 8311-8318.
13. J.-Q. Sha, X.-Y. Yang, Y. Chen, P.-P. Zhu, Y.-F. Song and J. Jiang, *ACS Applied Materials & Interfaces*, 2018, **10**, 16660-16665.
14. M.-T. Li, X.-Y. Yang, J.-S. Li, N. Sheng, G.-D. Liu, J.-Q. Sha and Y.-Q. Lan, *Inorganic Chemistry*, 2018, **57**, 3865-3872.
15. X. Li, K.-F. Zhou, Z.-B. Tong, X.-Y. Yang, C.-Y. Chen, X.-H. Shang and J.-Q. Sha, *Chemistry – An Asian Journal*, 2019, **14**, 3424-3430.
16. Q. Huang, T. Wei, M. Zhang, L.-Z. Dong, A. M. Zhang, S.-L. Li, W.-J. Liu, J. Liu and Y.-Q. Lan, *Journal of Materials Chemistry A*, 2017, **5**, 8477-8483.
17. Y. Yue, Y. Li, Z. Bi, G. M. Veith, C. A. Bridges, B. Guo, J. Chen, D. R. Mullins, S. P. Surwade, S. M. Mahurin, H. Liu, M. P. Paranthaman and S. Dai, *Journal of Materials Chemistry A*, 2015, **3**, 22989-22995.
18. D. Ma, L. Liang, W. Chen, H. Liu and Y.-F. Song, *Advanced Functional Materials*, 2013, **23**, 6100-6105.
19. S.-C. Huang, C.-C. Lin, C.-W. Hu, Y.-F. Liao, T.-Y. Chen and H.-Y. Chen, *Journal of Power Sources*, 2019, **435**, 226702.
20. W. Chen, L. Huang, J. Hu, T. Li, F. Jia and Y.-F. Song, *Physical Chemistry Chemical Physics*, 2014, **16**, 19668-19673.